Supplement of

Characterization of aerosol properties at Cyprus, focusing on cloud condensation nuclei and ice nucleating particles

Xianda Gong[1], Heike Wex[1], Thomas Müller[1], Alfred Wiedensohler[1], Kristina Höhler[2], Konrad Kandler[3], Nan Ma[1], Barbara Dietel[2], Thea Schiebel[2], Ottmar Möhler[2], and Frank Stratmann[1]

[1]Experimental Aerosol and Cloud Microphysics Department, Leibniz Institute for Tropospheric Research, Leipzig, Germany
[2]Institute for Meteorology and Climate Research – Atmospheric Aerosol Research, Karlsruhe Institute of Technology, Karlsruhe, Germany
[3]Institute for Applied Geosciences, Technical University Darmstadt, Darmstadt, Germany

Correspondence: Xianda Gong (gong@tropos.de)

S1 Instrumentation

As shown in Fig. S1.

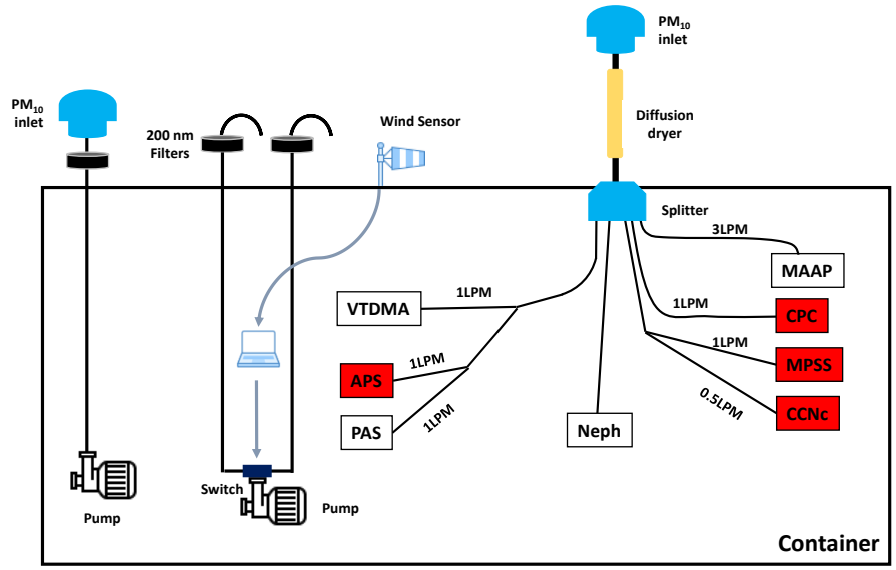

Figure S1. A schematic diagram of the measurement system and flow rate partitioning to the measurement devices. Indicated by the word "Switch" is a computer-based system that switched between two filters according to wind directions. The on-line instruments discussed in this paper are marked with red background. MPSS, APS and CCNc represent Mobility Particle Size Spectrometer, Aerodynamic Particle Sizer and Cloud Condensation Nuclei counter, respectively.

S2 Accounting for particle losses

The particle losses related to the transport of aerosol particles within the inlet tube system are determined using the Particle Loss Calculator (PLC) (von der Weiden et al., 2009). Size-dependent particle losses due to diffusion, sedimentation, turbulent inertial deposition, inertial deposition in a bend, and inertial deposition in a contraction are accounted for. The result is shown in Fig. S2, which depicts particle losses in % as a function of particle size.

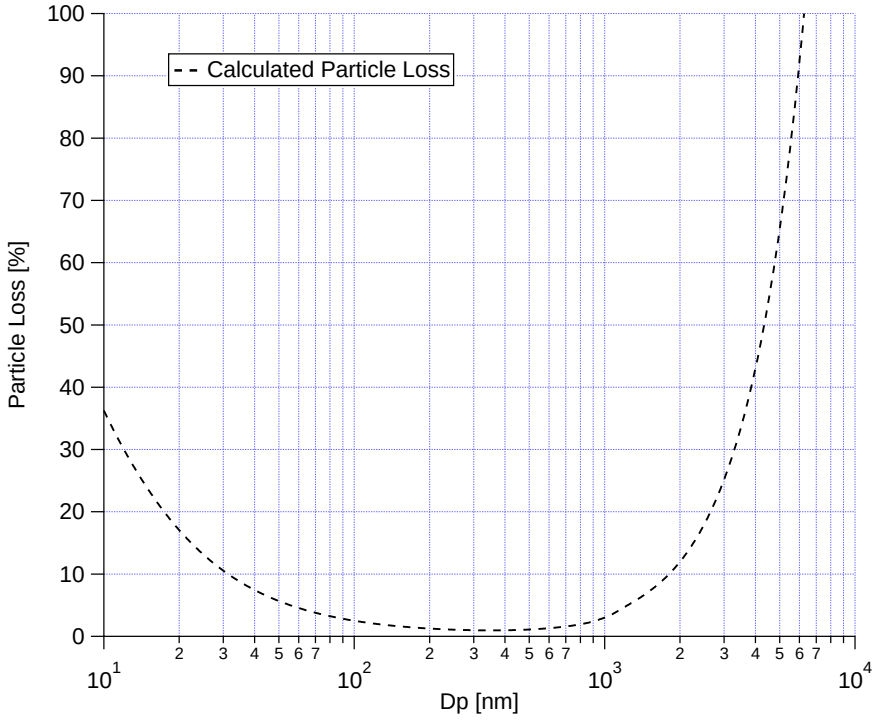

Figure S2. Size-dependent particle loss through the inlet.

S3 Filter sample information

Table S1. The information of TROPOS filter samples, including the sample number, start time, start flow, stop time, end flow, duration and status.

Sample number	Start time (UTC)	Start flow (L min^{-1})	Stop time (UTC)	End flow (L min^{-1})	Duration (h)	Status
Sample 01	2017/04/06 07:50:00	10.76	2017/4/09 06:10:00	9.95	23.07	Ocean sector
Sample 02	-	-	-	-	-	Blind filter
Sample 03	2017/04/07 09:50:00	10.00	2017/4/09 06:10:00	7.92	26.09	Land sector
Sample 04	2017/04/09 07:30:00	10.61	2017/4/14 06:30:00	12.10	23.76	Ocean sector
Sample 05	2017/04/09 07:30:00	9.85	2017/4/10 06:20:00	8.74	22.63	Land sector
Sample 07	2017/04/11 07:00:00	9.73	2017/4/12 06:30:00	8.89	22.00	Land sector
Sample 08	2017/04/12 07:00:00	9.86	2017/4/14 06:30:00	8.68	25.65	Land sector
Sample 09	2017/04/14 07:50:00	9.83	2017/4/18 07:10:00	4.19	20.65	Ocean sector
Sample 10	2017/04/14 07:50:00	9.55	2017/4/15 06:20:00	6.11	21.04	Land sector
Sample 11	2017/04/15 06:40:00	9.80	2017/4/16 06:40:00	8.79	23.73	Land sector
Sample 12	2017/04/16 07:00:00	9.67	2017/4/18 11:00:00	7.74	18.21	Land sector
Sample 13	2017/04/18 07:30:00	9.68	2017/4/21 08:00:00	8.4	20.87	Ocean sector
Sample 14	2017/04/18 11:20:00	9.60	2017/4/19 09:40:00	8.12	18.12	Land sector
Sample 15	2017/04/19 09:50:00	9.49	2017/4/20 09:20:00	9.07	19.83	Land sector
Sample 16	2017/04/20 09:40:00	9.70	2017/4/22 06:30:00	9.34	26.20	Land sector
Sample 17	-	-	-	-	-	Blind filter
Sample 18	2017/04/22 06:40:00	9.74	2017/4/23 06:20:00	8.28	22.20	Land sector
Sample 19	2017/04/23 06:40:00	9.53	2017/4/24 06:20:00	7.95	23.05	Land sector
Sample 20	2017/04/24 06:40:00	9.65	2017/4/25 06:20:00	8.08	23.61	Land sector
Sample 21	2017/04/25 06:40:00	9.65	2017/4/26 09:40:00	8.71	20.42	Land sector
Sample 22	2017/04/26 09:50:00	9.65	2017/4/27 06:50:00	8.91	20.95	Land sector
Sample 23	2017/04/27 07:00:00	9.67	2017/4/28 06:30:00	8.11	22.95	Land sector
Sample 24	2017/04/28 06:40:00	9.57	2017/4/29 06:20:00	6.67	23.16	Land sector

Table S2. The information of KIT filter samples, including the sample number, start time, stop time, flow and duration.

Sample number	Start time (UTC)	Stop time (UTC)	Flow (L min^{-1})	Duration (h)
Sample01	2017/04/02 13:00:00	2017/04/02 17:00:00	15	4.00
Sample02	2017/04/03 07:08:00	2017/04/03 15:13:00	15	8.08
Sample04	2017/04/04 07:29:00	2017/04/04 15:17:00	15	7.80
Sample06	2017/04/05 07:34:00	2017/04/05 15:36:00	15	8.03
Sample08	2017/04/06 08:06:00	2017/04/06 13:58:00	15	5.87
Sample10	2017/04/07 07:31:00	2017/04/07 15:40:00	15	8.15
Sample11	2017/04/08 08:20:00	2017/04/08 16:20:00	15	8.00
Sample12	2017/04/09 09:35:00	2017/04/09 17:35:00	15	8.00
Sample13	2017/04/10 07:30:00	2017/04/10 15:30:00	15	8.00
Sample14	2017/04/11 08:30:00	2017/04/11 16:30:00	15	8.00
Sample15	2017/04/12 07:35:00	2017/04/12 15:35:00	15	8.00
Sample16	2017/04/13 07:35:00	2017/04/13 15:35:00	15	8.00
Sample17	2017/04/14 07:35:00	2017/04/14 15:35:00	15	8.00
Sample18	2017/04/15 07:35:00	2017/04/15 15:35:00	15	8.00
Sample19	2017/04/16 07:35:00	2017/04/16 15:35:00	15	8.00
Sample20	2017/04/17 07:43:00	2017/04/17 15:43:00	15	8.00
Sample21	2017/04/18 07:43:00	2017/04/18 15:43:00	15	8.00
Sample22	2017/04/19 07:43:00	2017/04/19 15:43:00	15	8.00
Sample23	2017/04/20 07:43:00	2017/04/20 15:43:00	15	8.00
Sample24	2017/04/21 07:43:00	2017/04/21 15:43:00	15	8.00
Sample25	2017/04/22 06:55:00	2017/04/22 14:20:00	15	7.42
Sample27	2017/04/23 07:15:00	2017/04/23 15:15:00	15	8.00
Sample28	2017/04/24 06:42:00	2017/04/24 14:42:00	15	8.00
Sample30	2017/04/25 07:26:00	2017/04/25 15:26:00	15	8.00
Sample32	2017/04/26 07:32:00	2017/04/26 15:32:00	15	8.00

S4 Wind speed and direction

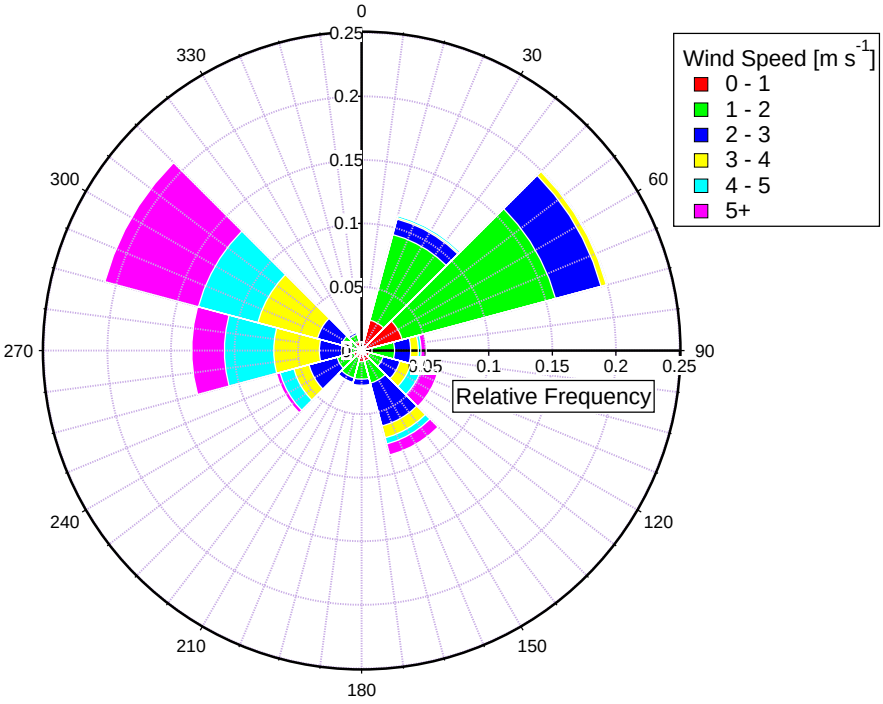

Figure S3. Wind rose based on 10 minutes mean of wind speed and direction measured at the station for whole campaign.

S5 Correlation of NO_x and N_{total}

Fig. S4 shows the scatter plot of N_{total} against NO_x. A good correlation (R^2=0.62) was found between extremely high concentrations of NO_x and N_{total} (upper panel in Fig. S4). No correlation was observed at lower concentrations of NO_x and N_{total} (lower panel in Fig. S4).

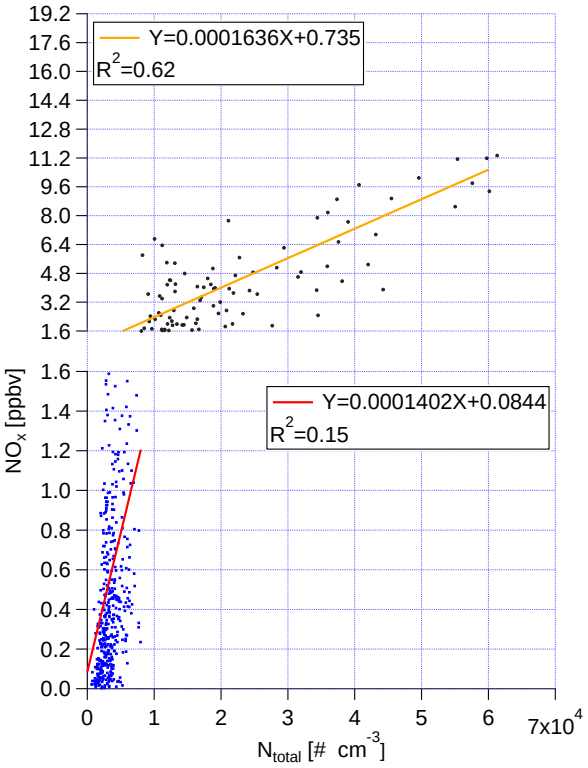

Figure S4. Scatter plot of N_{total} versus NOx. R^2 and fitting function are given in the panels.

S6 Identification of pollution periods

Fig. S5 shows the measured super-micron PNSDs as contour plot, together with NO_x information from 06:00 UTC 16 to 00:00 UTC 18 April. Pollution events were identified based on the PNSDs. The criteria are, first of all, the appearance of a distinct ultrafine particle mode with a dN/dlogDp value large than 3000 cm^{-3} at 15 nm. Secondly, the ultrafine particle mode featured similar PNSDs, without any sign of growth.

The resulting PNSDs during the pollution events featured a pronounced mode with a maximum at about 15 nm (median dN/dlogDp value larger than 10^4 cm^{-3}). Three pollution periods were observed in the example shown here, i.e., from 18:10

to 22:20 UTC 16 Apr, 04:50 to 05:10 UCT, 17:30 to 20:50 UTC 17 Apr. During the pollution periods, high concentrations of NO_x were also observed.

Once we identified all the pollution periods. We made the wind rose plot for all the pollution periods, as shown in Fig. S6.

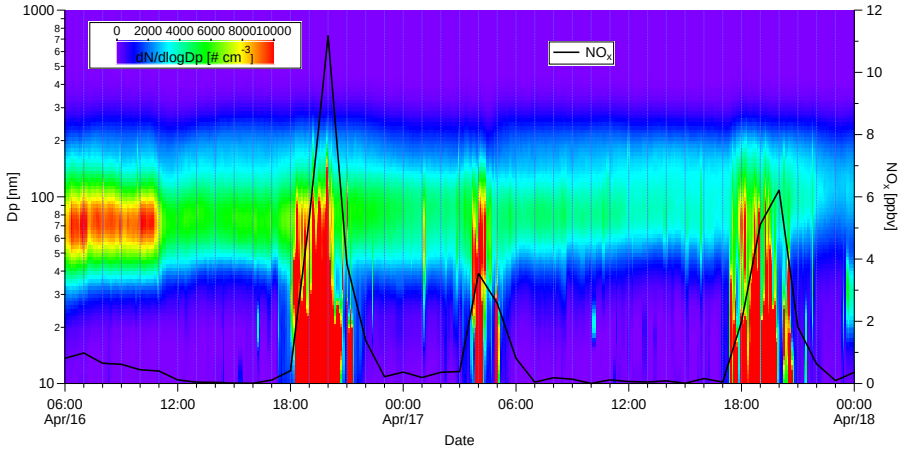

Figure S5. Contour plots for PNSDs from 06:00 UTC 16 to 00:00 UTC 18 April. Black line shows time series of NO_x concentration.

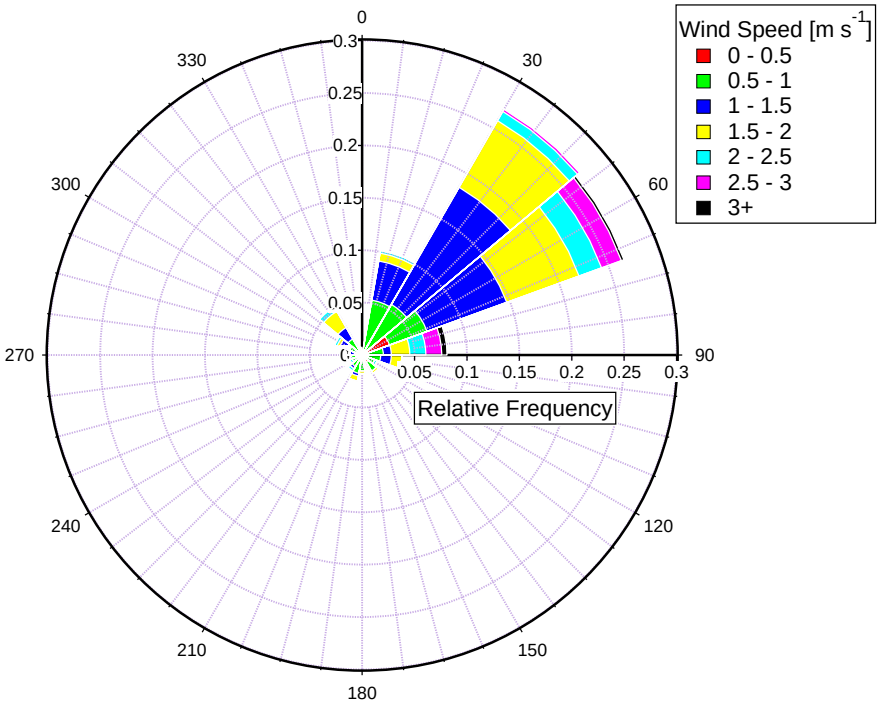

Figure S6. Wind rose based on 10 minutes average of wind speed and direction measured at the station for pollution periods.

S7 Filter background and measurement uncertainty

As shown in Fig. S7, the background of LINA and INSEKT measurement is tested. The ultrapure water droplets started to freeze at -20 °C. Compared to the ultrapure water, the frozen fraction (f_{ice}) curve from blind filters washed with ultrapure water is shifted approx 1 °C towards higher temperatures. The f_{ice} curves determined for atmospheric filter samples are clearly above those obtained for the blind filters, while the f_{ice} of 225- and 3375-fold dilutions of the filter washing water is close to that of ultrapure water.

For the subtraction of background, we used the same method as proposed by Umo et al. (2015). Thereto, the cumulative concentration of INP per air volume determined for the blind filters (KT_{blind}) was subtracted from that for filter samples (KT_{filter}):

$$N_{\text{INP}} = KT_{\text{filter}} - KT_{\text{blind}} \tag{1}$$

Based on Agresti and Coull (1998), the confidence interval of f_{ice} can be calculated by:

$$\left(f_{\text{ice}} + \frac{z_{\alpha/2}^2}{2n} \pm z_{\alpha/2}\sqrt{[f_{\text{ice}}(1-f_{\text{ice}}) + z_{\alpha/2}^2/(4n)]/n}\right) / \left(1 + \frac{z_{\alpha/2}^2}{n}\right) \tag{2}$$

where $z_{\alpha/2}^2$ is the standard score at a confidence level $\alpha/2$, which for a 95% confidence interval is 1.96. n is the droplet number of each experiment.

The uncertainty of N_{INP} is calculated based on the uncertainty of the f_{ice} as we outlined above. The error bar in Fig. S8 represents 95% confidence interval for N_{INP}.

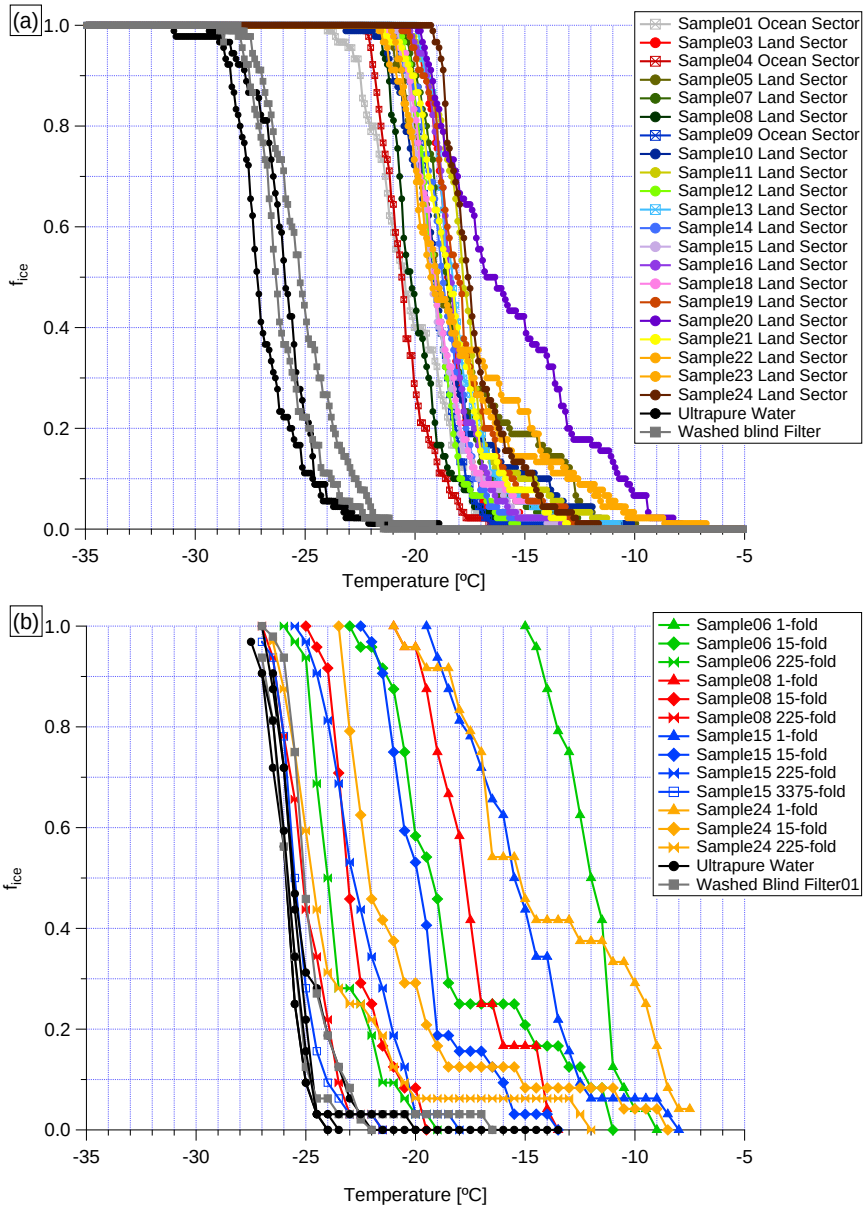

Figure S7. The f_{ice} of washed filter samples, together with background signals of ultrapure water and ultrapure water washed blind filter samples of LINA (a) and INSEKT (b) measurement results. For INSEKT, only a subset of all samples is shown exemplarily, to enable seeing curves for the same sample from different dilutions.

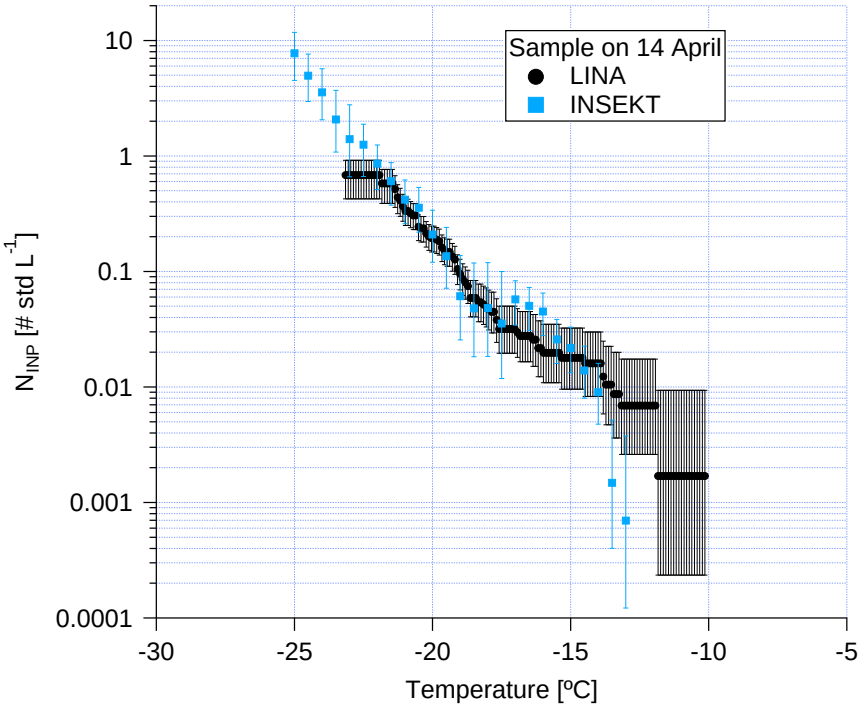

Figure S8. N_{INP} measured by LINA (black) and INSEKT (blue) as a function of temperature. For comparison, the LINA and INSEKT results here were both sampled on 14 April. The error bar shows the 95% confidence interval in N_{INP}.

S8 INSEKT measured N_{INP} against the ratio of time sampling from the ocean sector

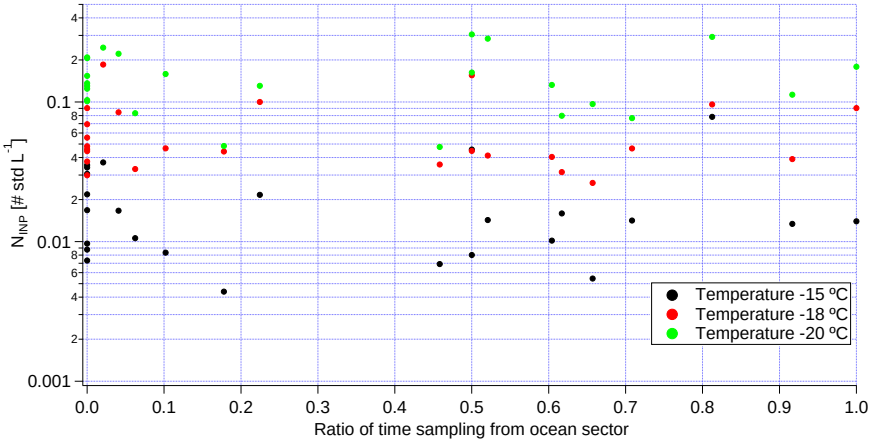

Figure S9. Scatter plot of N_{INP} (measured by INSEKT) versus the ratio of time sampling from the ocean sector at −15, −18 and −20 °C.

S9 Log-normal distribution of N_{INP} test

Here we used two methods to test our N_{INP} frequency distributions. The quantile-quantile plot was originally proposed by Wilk and Gnanadesikan (1968) to compare two distributions by plotting quantiles of one versus quantiles of the other. Here, we plot logarithmic N_{INP} at −18 °C versus a standard normal distribution, as shown in Fig. S10. The measured N_{INP} is close to the reference line, indicating that the N_{INP} follows the log-normal distribution. Note that the quantile-quantile plot provides only a rough measure how similar the compared distributions are.

Table S3. Lillifors test results.

Temperature	LINA		INSEKT	
	h	p	h	p
−15 °C	0	0.3455	0	0.4461
−18 °C	0	0.1810	0	0.1400
−20 °C	0	0.0355	0	0.5000

Furthermore, we used the Lilliefors test (Lilliefors, 1967) to determine if the observed N_{INP} frequency distributions follow a log-normal distribution. In statistics, the Lilliefors test is a normality test based on the Kolmogorov-Smirnov test (Sachs, 2012). It is used to test the null hypothesis of the data following a normal distribution, with the null hypothesis not including the actual

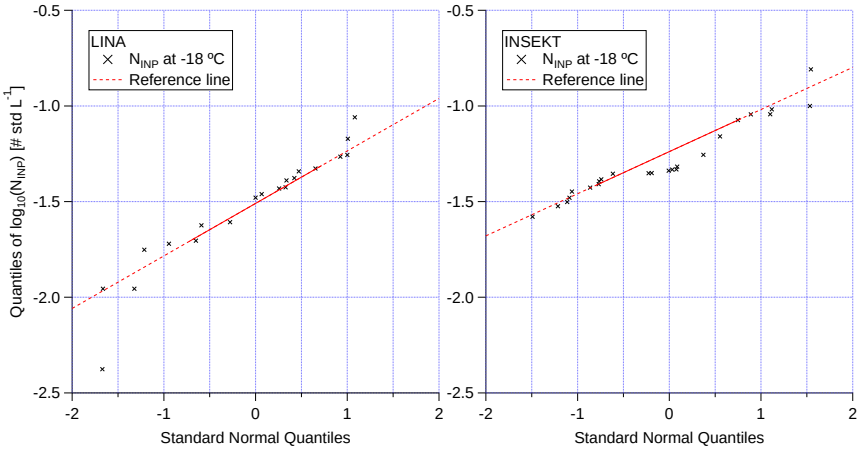

Figure S10. The quantile-quantile plot of logarithmic N_{INP} measured by LINA and INSEKT at -18 °C with a random normal distribution.

parameters (mean and standard deviation) of the normal distribution. Results (h-value and p-value) of the carried out Lilliefors tests are shown in Tab. S3. A return value of h = 0 indicates that the logarithmic N_{INP} (measured by LINA and INSEKT) follow normal distributions at -15, -18 and -20 °C. As log-normally distributed N_{INP} are indicative for the observed INP population having undergone a series of random dilutions while being transported (Welti et al., 2018), the performed Lilliefors tests yield additional prove for the INP sampled during our measurements originating from long-range transport rather than local sources.

S10 Correlation of N_{INP} with particle number/surface area concentration

Table S4. Coefficient of determination (R^2) of LINA and INSEKT measured N_{INP} with $N_{>500\mathrm{nm}}$.

Temperature	LINA	INSEKT
-15 °C	0.0877	0.0277
-18 °C	0.2369	0.0602
-20 °C	0.0950	0.0006

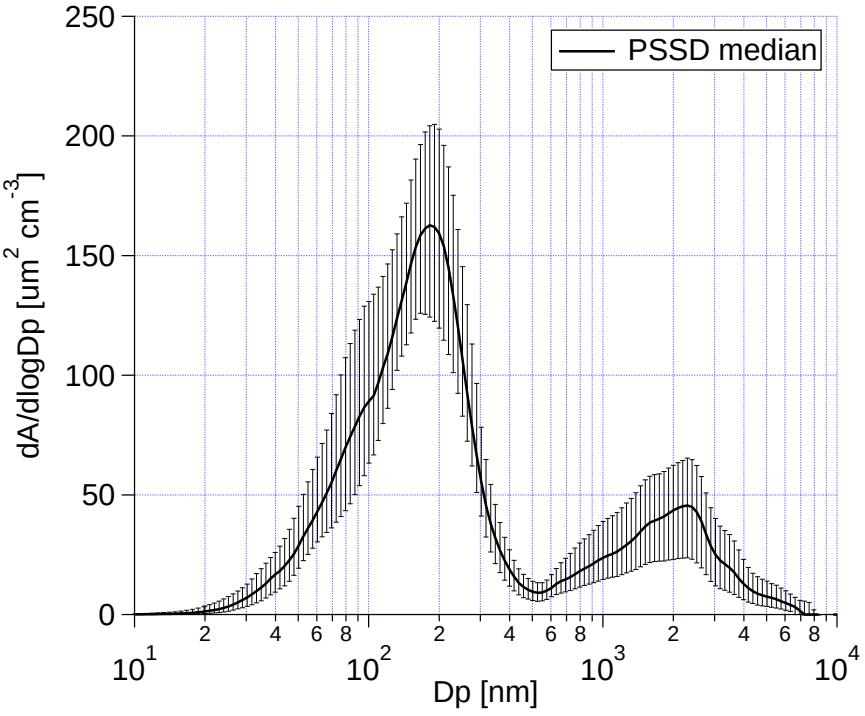

Figure S11. The median PSSD (excluding airport pollution period) during the whole campaign. The error bar indicates the range between the 25 % and 75 % percentiles.

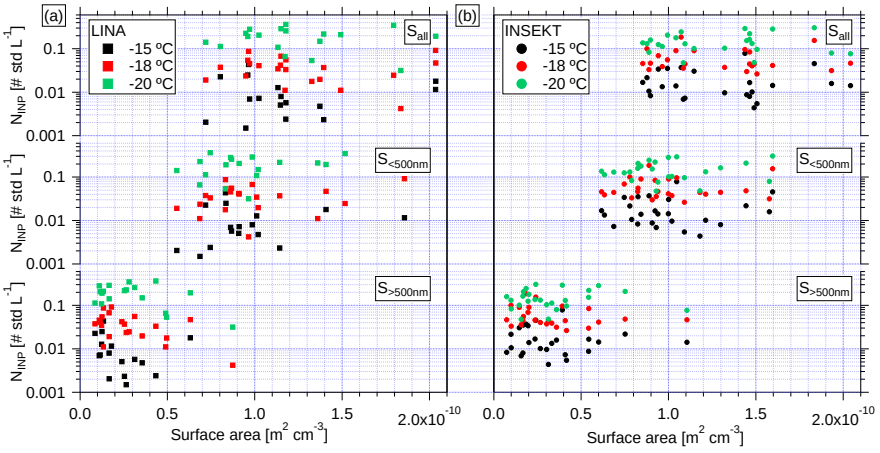

Figure S12. Scatter plot of N_{INP} (measured by LINA (a) and INSEKT (b)) against S_{all}, S_1, S_2 at −15, −18 and −20 °C.

Table S5. R^2 of LINA and INSEKT measured N_{INP} with particle surface area concentration.

Temperature	LINA			INSEKT		
	S_{all}	S_1	S_2	S_{all}	S_1	S_2
−15 °C	0.0009	0.0011	0.0319	0.0016	0.0153	0.0055
−18 °C	0.0002	0.0905	0.1945	0.0059	0.0079	0.0521
−20 °C	0.0001	0.0852	0.1255	0.0395	0.0362	0.0057

References

Agresti, A. and Coull, B. A.: Approximate is Better than "Exact" for Interval Estimation of Binomial Proportions, The American Statistician, 52, 119–126, https://doi.org/10.1080/00031305.1998.10480550, https://doi.org/10.1080/00031305.1998.10480550, 1998.

Lilliefors, H. W.: On the Kolmogorov-Smirnov Test for Normality with Mean and Variance Unknown, Journal of the American Statistical Association, 62, 399–402, https://doi.org/10.1080/01621459.1967.10482916, https://amstat.tandfonline.com/doi/abs/10.1080/01621459.1967.10482916, 1967.

Sachs, L.: Applied statistics: a handbook of techniques, Springer Science & Business Media, 2012.

Umo, N., Murray, B., Baeza-Romero, M., Jones, J., Lea-Langton, A., Malkin, T., O'Sullivan, D., Neve, L., Plane, J., and Williams, A.: Ice nucleation by combustion ash particles at conditions relevant to mixed-phase clouds, Atmospheric Chemistry and Physics, 15, 5195–5210, 2015.

von der Weiden, S. L., Drewnick, F., and Borrmann, S.: Particle Loss Calculator - a new software tool for the assessment of the performance of aerosol inlet systems, Atmos. Meas. Tech., 2, 479–494, https://doi.org/10.5194/amt-2-479-2009, http://www.atmos-meas-tech.net/2/479/2009/, 2009.

Welti, A., Müller, K., Fleming, Z. L., and Stratmann, F.: Concentration and variability of ice nuclei in the subtropical maritime boundary layer, Atmospheric Chemistry and Physics, 18, 5307–5320, 2018.

Wilk, M. B. and Gnanadesikan, R.: Probability plotting methods for the analysis for the analysis of data, Biometrika, 55, 1–17, https://doi.org/10.1093/biomet/55.1.1, http://dx.doi.org/10.1093/biomet/55.1.1, 1968.